WAVE EVOLUTION ON A FALLING FILM

Hsueh-Chia Chang

Department of Chemical Engineering, University of Notre Dame, Notre Dame, Indiana 46556

INTRODUCTION

Since the pioneering experiment by the father-son team of the Kapitza family during their house arrest in the late forties (Kapitza & Kapitza 1949), wave evolution on a falling film has intrigued many researchers. One of its main attractions is its simplicity—it is an open-flow hydrodynamic instability that occurs at very low flow rates. It can hence be studied with the simplest experimental apparatus, an obviously important factor for the Kapitzas. Yet, it yields a rich spectrum of fascinating wave dynamics, including a very unique and experimentally well-characterized sequence of nonlinear secondary transitions that begins with a selected monochromatic disturbance and leads eventually to nonstationary and broad-banded (in both frequency and wave number) "turbulent" wave dynamics. (Turbulence here is used interchangeably with irregular spatio-temporal fluctuations.) While this transition to "interfacial turbulence" or "spatio-temporal chaos" seems to be quite analogous to other classical instabilities at first glance, there are subtle but important differences that have recently come to light. The pertinent nonlinear mechanisms behind these secondary transitions are the focus of the present review.

We shall be mostly concerned with transitions on a free-falling vertical film. Wave dynamics on an inclined plane is quite analogous to the vertical limit and most experiments and theories have focused on the latter. For the vertical film, the problem is defined by two independent dimensionless parameters and we prefer the Russian convention of using the Reynolds

103

number $R = \langle u \rangle h_N / v$ and the Kapitza number $\gamma = \sigma / \rho v^{4/3} g^{1/3}$ where $\langle u \rangle$ is the average velocity, h_N is the Nusselt flat-film film thickness such that $h_N \langle u \rangle$ is the flow rate per unit width and $\langle u \rangle = g h_N^2 / 3v$, v the kinematic viscosity, ρ the density, σ the interfacial tension and g the gravitational acceleration. If one uses the "natural" scalings on the full Navier-Stokes equation, the resulting two parameters would be R and the Weber number $W = \sigma / \rho \langle u \rangle^2 h_N$ which are the ones used in some literature. However, the Kapitza number offers the advantage that it is only a function of the physical properties of the liquid and not the flow rate. (For water, $\gamma = 2850$ at 15°C.) The two conventions are interchangeable by $\gamma = W R^{5/3} / 3^{1/3}$.

At very large Reynolds numbers ($R > 1000$), the waves observed on the falling film are of the shear-wave variety with wavelengths comparable to or shorter than h_N. [See the linear stability analysis of Floryan et al (1987) and the experiment of Bertschy et al (1983) for inclined films.] Such high-flow-rate conditions typically yield turbulent films (turbulent in the classical sense) dominated by internal Tollmien-Schlichting disturbances. The interfacial dynamics is simply enslaved by the internal turbulence. At moderately high R ($300 < R < 1000$), long interfacial waves characteristic of gravity-capillary instabilities begin to appear (Chu & Dukler 1974). However, the wave dynamics is extremely nonstationary, especially for the persisting short waves which seem to be generated by a vortex shedding mechanism from the long waves. At extremely low flow rates ($R \ll 1$), the film becomes so thin that intermolecular forces and contact line dynamics become important as the film ruptures. We are concerned with the intermediate region ($1 < R < 300$) such that the instability consists of long interfacial waves dominated by gravity-capillary effects.

Wave evolution by natural excitation in this region of Reynolds numbers is shown in the schematic of Figure 1. Four distinct wave regions have been observed. In the inception region (region I), infinitesimal disturbances at the inlet are amplified downstream to form a monochromatic wave at the end of the region, indicating that the instability is a convective one and not of the absolute variety. If the initial disturbance is sufficiently monochromatic in frequency, the emerging wave inherits the forcing frequency. If the disturbance has a wide band of frequency, as is true with natural noise, a highly selective linear filtering process in region I yields a unique monochromatic wave field for all wide-band disturbances. In particular, transverse disturbances are selectively damped in this inception region. Within this region, the amplitude of the monochromatic wave grows exponentially downstream as in all linear excitation processes of convectively unstable systems. Beginning in region II, however, the exponential growth is arrested by weakly nonlinear effects as the amplitude of the monochromatic wave saturates to a finite value dependent on the wave
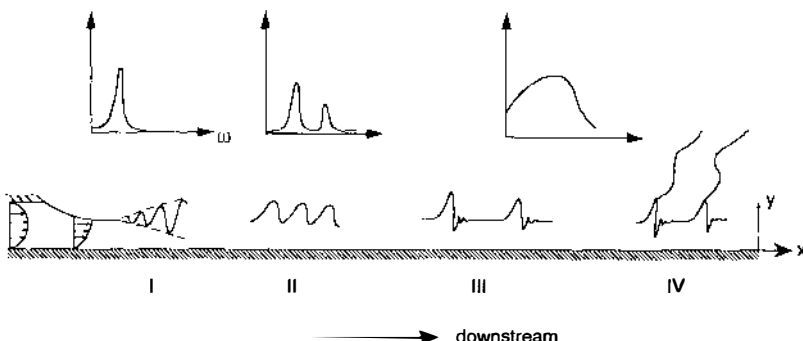
Figure 1 Schematic of the four wave regimes in a naturally excited evolution on a falling film from a slit. The wave spectra from localized probes at the four regions are also shown. The parameter ω is the wave frequency. For higher R values ($R > 50$), region III may not be present.

number, R, and γ. Due to this weakly nonlinear interaction between an unstable fundamental Fourier mode and a stable second harmonic, the monochromatic wave of region I begins to develop a finite overtone in region II as its sinusoidal shape steepens downstream. There is also a negative nonlinear correction to the wave speed of the inception region such that the waves actually slow down as they grow (Lin 1983). Some experimental evidence indicates that even the wave number of the saturated periodic wave exiting from region II, which is still a very uniform wave field, is different from that of the monochromatic wave emerging from region I due to a nonlinear selection mechanism. In a periodically forced experiment with a sufficiently large forcing amplitude, both region I and region II may be bypassed and the first uniform wave field that emerges contains large-amplitude waves whose wave frequencies are close to the forcing frequency except at very low values (Kapitza & Kapitza 1949, Alekseenko et al 1985). The periodic finite-amplitude disturbances in a forced experiment can hence entrain waves that would not have been selected by the linear and nonlinear selection mechanisms of regions I and II. For small-amplitude and broad-banded natural or artificially introduced disturbances, however, the uniform wave fields emerging from regions I and II are independent of the disturbances present. They are uniquely selected by the linear and nonlinear mechanisms in regions I and II.

Both finite-amplitude wave fields generated by periodic forcing and naturally excited wave fields emerging from region II travel a long distance (~ 10 wavelengths) in a stationary manner, e.g. without visible changes in

their shape or speed, before they undergo another slow evolution in region III. Here, two dominant instabilities of the finite-amplitude waves have been observed. The best data are recorded by Liu & Gollub (1993) although they are taken for inclined films. Neighboring waves coalesce at intermittent locations due to a subharmonic instability (Prokopiou et al 1991) or a long-wave modulation appears characteristic of sideband instabilities (Cheng & Chang 1992a). These two instabilities create intermittent patches of defects to the otherwise uniform field of waves. Within these patches, the distorted waves grow in wavelength, amplitude, and speed and evolve into characteristic spatially localized teardrop humps. These humps have steep fronts which are relaxed by a series of front-running bow waves whose wavelength is close to the monochromatic waves at inception. These larger and faster humps begin to expand the patches in the downstream direction as they overtake the original slower waves, so much so that all of the latter may vanish eventually. The wave frequency or wave number spectrum now becomes very broad, in contrast to the monochromatic spectrum in region I and the fundamental-overtone pair in region II. This, however, does not imply that a continuous band of dispersive waves dominate the interface as in turbulent channel flow. Instead, a large portion of the band is locked into the characteristic hump of the evolved waves and travels in synchrony. The broad-banded spectrum is due mostly to the localized shape of the humps which is strikingly identical. These robust humps have a characteristic length that is much shorter than the typical separation between humps where the film is essentially flat. They are hence referred to as *solitary waves*, or more appropriately, *solitary humps*. The separation between the individual humps are typically nonuniform and time-varying, indicating nonstationary interaction among them and reflecting the spatio-temporal irregularity of their births. However, the humps themselves remain nearly identical and do not alter their shape significantly during the interaction within region III.

Finally, in region IV, transverse variation begins to develop on the wave crests of the solitary humps. The dynamics of the transverse variation is nonstationary and these transverse variations grow to such amplitude (not in height but in the direction parallel to the wall) that adjacent crests merge at various points and pinch off. However, the wave shape in the flow direction (x in Figure 1) retains the solitary shape except near the pinch points. For vertical water films at low R, regions I to III occupy 30 to 40 inception wavelengths with each region spanning about 10 wavelengths. (The wavelength selected at inception is about 1 cm for water at the Reynolds number of interest.) Region IV seems to persist indefinitely downstream. If the introduced disturbance at the feed, or elsewhere in the channel, contains significant transverse variation such that it is not entirely

filtered in the inception region I, then region III may be negligible in length or may be skipped entirely.

MODEL EQUATIONS AND WAVE INCEPTION

Although the wave transition sequence shown in Figure 1 seems to be quite similar to transitions in other classical hydrodynamic instabilities like free-convection boundary layer and shear instabilities in channel flow, there are several important factors that make this instability unique and also render it more amenable to analysis. It could well be the first transition sequence to be fully understood. The first factor is the difference in the streamwise and normal length scales. In all regions in Figure 1 and for $R < 300$, the film height at the wave crest never exceeds $1/10$ of the characteristic wavelength or the characteristic length of the solitary humps. At low R, this long-wave characteristic of the interfacial disturbances motivates a lubrication-type expansion with respect to the "film parameter" ε defined as the ratio between the characteristic wave height and the characteristic wavelength. This long-wave expansion yields the following evolution equation

$$\frac{\partial h}{\partial t} + 3h^2 h_x + \left(\frac{4}{5} R h^6 h_x + \frac{RWh^3}{3} h_{xzz} + \frac{RWh^3}{3} h_{xxx} \right)_x$$
$$+ \frac{RW}{3} (h^3 h_{zzz} + h^3 h_{zxx})_z = 0, \quad (1)$$

where the characteristic length and time used to nondimensionalize the variables are h_N and $h_N/\langle u \rangle$, respectively. In a more popular version of this equation, the interfacial velocity is used in the time scale. This corresponds to multiplying all coefficients in (1) except the first one by a factor of $2/3$. In this other version $RW/3$ is also replaced by a different Weber number $W' = \sigma/\rho h_N^2 g$. Roskes (1970) is responsible for the $O(\varepsilon^2)$ version of (1) for strong surface-tension fluids $[W \sim O(\varepsilon^{-2})]$. Dispersion, which will be shown to be important in both the linear and nonlinear instability mechanisms, has been omitted in the equation. It was, however, included in a higher-order equation that Nakaya (1975) derived for both $W \sim O(\varepsilon^0)$ and $W \sim O(\varepsilon^{-2})$. Lower-order equations, for various relative orders of W with respect to ε, have been derived by different investigators beginning with the work of Benney (1966). All these evolution equations, however, require the Reynolds number to be $O(\varepsilon^0)$, corresponding to lubrication-flow conditions.

Further simplification of (1) is possible by carrying out an expansion in

the amplitude η, where $h = 1 + \eta$. This weakly nonlinear expansion for strong surface-tension fluids was first carried out by Lin (1974) and Nepomnyaschy (1974) independently for falling-film waves and it yields the following $O(\eta^2)$ equation for two-dimensional waves without z variation, known as the Kuramoto-Sivashinsky (KS) equation:

$$H_t + 4HH_x + H_{xx} + H_{xxxx} = 0, \tag{2}$$

where both R and W have been conveniently absorbed by the moving-coordinate, slow-time, long-wave, and small-amplitude expansion:

$$t = \tau\left(\frac{48R}{25W}\right), \quad \eta = 4\left(\frac{8R}{25W}\right)\left(\frac{5W}{12}\right)^{1/2} H,$$

and

$$x \to \left(\frac{5W}{12}\right)^{1/2}(x - 3t).$$

The parameter-independent property of the KS equation and its simplicity in retaining only the most dominant nonlinear term HH_x, which arises from interfacial kinematics in the present problem, have made it a popular generic model for numerical and mathematical scrutiny.

One should, however, be cognizant of the assumptions that have been made in deriving both (1) and (2). The former assumes a small wave height to wavelength ratio ε and $R \sim O(\varepsilon^0)$ while the latter imposes the additional stipulation that the deviation amplitude $\eta = h - 1$ must be small. Note that the small η approximation is much stronger than the small-ε long-wave approximation since the wave height can be small relative to the wavelength and still be the same order or larger than the Nusselt film thickness h_N or the average film thickness. The observed waves typically obey the long-wave approximation but not necessarily the small-amplitude assumption. Both equations are also strictly valid only for strong surface-tension fluids unless higher order terms are added to (1). Nevertheless, with careful consideration concerning their validity, they can be welcomed substitutes for the full Navier-Stokes equation since the latter is still beyond exhaustive numerical analysis. (See, however, the recent work of Kheshgi & Scriven 1987 and Ho & Patera 1990. There is also an ongoing effort at MIT.)

Extensive numerical analysis of the "strongly" nonlinear equation in (1) has been carried out by Pumir et al (1983) and by the Northwestern group (Joo et al 1991; Joo & Davis 1992a,b). Pumir et al first demonstrated and Rosenau et al (1991) and Joo et al (1991) recently confirmed that finite-time blow-up and wave breaking, which violate the small ε long-wave expansion, are often encountered during the integration of (1). Since the

actual film does not exhibit such behavior, the strongly nonlinear evolution equation in (1) must have omitted certain important nonlinear growth-arresting mechanisms in its long-wave expansion. On the other hand, one can easily show by the energy method that the KS equation (2), with reasonable boundary conditions, always yields bounded solutions for all time. Since the small-amplitude evolution of (1) is also described by (2), while the large-amplitude evolution of (1) quite often yields blow-up solutions that are not consistent with the long-wave expansion, the advantage of the more complex evolution equation over the KS equation is rather limited.

For $R \gg 1$, both (1) and (2) are definitely not valid and the only available simplification of the Navier-Stokes equation is offered by the boundary-layer equation (BL) first studied by Shkadov et al (1970). Unlike the derivation that leads to (1) and (2), the BL equation is derived with only the long-wave expansion without overly restrictive stipulations on the order for R, W, and the deviation wave amplitude η (Chang et al 1993a). Inertia-induced instability and dispersion are fully captured. The BL equation is

$$\frac{\partial u}{\partial t} + u\frac{\partial u}{\partial x} + v\frac{\partial u}{\partial y} = \frac{1}{5\delta}\left(h_{xxx} + h_{xzz} + \frac{1}{3}\frac{\partial^2 u}{\partial y^2} + 1\right)$$

$$\frac{\partial w}{\partial t} + u\frac{\partial w}{\partial x} + v\frac{\partial w}{\partial y} + w\frac{\partial w}{\partial z} = \frac{1}{5\delta}\left(h_{xxz} + h_{zzz} + \frac{1}{3}\frac{\partial^2 w}{\partial y^2}\right)$$

$$\frac{\partial u}{\partial x} + \frac{\partial v}{\partial y} + \frac{\partial w}{\partial z} = 0 \tag{3}$$

$$y = h(x, z) \quad h_t = v - uh_x - wh_z \quad \frac{\partial u}{\partial y} = \frac{\partial w}{\partial y} = 0$$

$$y = 0 \quad u = v = w = 0.$$

We have compared the linear stability result of (3) to the exact results of the full Orr-Sommerfeld equation and found it to be accurate for $R < 300$ for most realistic fluids (Chang et al 1993a). Unlike the KS equation which contains no explicit parameters, (3) yields a scaled Reynolds number

$$\delta = R^{11/9}/5\gamma^{1/3}3^{7/9}$$

which introduces the destabilizing and dispersive effects of inertia at higher flow rates. Nevertheless, it is still more convenient to study than the full Navier-Stokes equation which contains two parameters. At vanishing δ, it can be readily shown that (3) reduces to (1) and then to (2) if a proper

scaling for δ in terms of the film parameter is assigned. An ad hoc but convenient simplification of (3) can be made by arbitrarily assuming a self-similar parabolic flow profile beneath the film (Shkadov 1967, 1968). This reduces (3) to the greatly simplified form of the "integral boundary-layer" equation (IBL) or averaged equation for two-dimensional waves,

$$\frac{\partial q}{\partial t} + \frac{6}{5}\frac{\partial}{\partial x}(q^2/h) - \frac{1}{5\delta}(hh_{xxx}+h-q/h^2) = 0$$

$$\frac{\partial h}{\partial t} + \frac{\partial q}{\partial x} = 0 \qquad\qquad (4)$$

where $q = \int_0^h u\,dy$ is the volumetric flow rate per unit span width.

In numerical simulations of (3) and (4) (Demekhin & Shkadov 1985, Trifonov & Tsvelodub 1991, Chang et al 1993a), it is found that the boundary-layer or long-wave approximation is always obeyed, c.g. the blow-up behavior of (1) is never observed and ε remains small. This is true even at low δ conditions where (1) supposedly applies. We believe higher order ε terms omitted in (1) are responsible for arresting the blow-up phenomenon. This is supported by our effort to reduce Equation (3) to Equation (1) (Chang et al 1993a). Since there are now two small parameters, the dispersion δ and the "film" parameter ε, relative order between the two must be established. It is found that $\delta \sim O(\varepsilon^{2/3})$ for the reduction to (1). This is equivalent to assigning R and W orders in ε in the derivation of (1) and (2). Since ε is not really a free parameter but one determined by the solution, the reduction essentially permits large-amplitude solutions like blow-up solutions by artificially reducing the effect of δ-related mechanisms like dispersion. Equivalently, a blow-up solution of (1) would trigger higher order ε effects such as dispersion to suppress further growth. Since these terms are not included in (1), blow-up occurs. The weakly nonlinear version of the KS equation suppresses unbounded growth by limiting itself to small-amplitude evolutions of (1) that do not trigger blow up. Since dispersion and other higher order terms in ε are included in the BL equation—the order of δ is not stipulated to be artificially small at a specific order of ε, it yields the proper description of wave evolution even at low δ. (Quantitative agreement with measured wave tracings will be presented in the next section.) It should hence be considered the model equation of choice, short of the complete Navier-Stokes equation, for long waves at $R < 300$. Equations (1) and (2) should be reserved for small-amplitude waves at low δ. In this limit, the KS equation is a far simpler equation to study than Equation (1). Although the IBL equation is derived in an ad hoc manner, it yields the correct leading-order linear (Prokopiou et al 1991) and nonlinear (Trifonov &

Tsvelodub 1991, Tsvelodub & Trifonov 1992) behavior in the low-δ limit ($\delta < 0.05$). It is hence a good substitute for the KS equation to include dispersive waves and an excellent simplification of the BL equation at low δ.

The danger in a priori assigning relative orders of R, W, and η with respect to ε in a long-wave expansion was recognized by Benney (1966). He found that his weakly nonlinear theories yield either the Burger equation, the KdV equation, or others depending on the specific assignments made. Since R and W are independent parameters that specify the wave height and wavelength in ε, these a priori assignments often yield equations that cannot describe the full range of waves. As a result, shock formation for the Burger equation and blow-up solutions for others occur when these equations are integrated as the waves attempt to evolve into ones beyond their description. One should only assume ε is small without specifying the orders of R, W, and η as in the derivation of the BL equation.

Another welcomed feature of wave evolution on a falling film at $R < 300$ is the difference in time scale between the characteristic time of wave evolution and the wave period. This is seen in the locally stationary and uniform two-dimensional periodic waves in region II where the waves are nearly identical over 10 wavelengths and a particular crest can travel the same distance without changing its shape or speed appreciably. The evolution in region III is more localized in space, especially at the beginning of the region. Nevertheless, one can still see small patches of stationary waves that span one or two wavelengths. The solitary humps of regions III and IV are also stationary although the separation between them can often be time-varying. Even here, the fluctuations can probably be modeled as local dynamics near a periodic train of stationary solitary humps. It is hence quite reasonable to construct stationary periodic waves by a Lagrangian transformation $x \rightarrow x - ct$ and study the steady-state version of any of the model equations in the Lagrangian frame. This introduces an additional parameter, the wave speed c, but converts the initial value problem into a far simpler boundary value problem. Linear stability analysis and weakly nonlinear theories for the dynamics near these stationary waves can then determine which wave will be selected in the various transitions. In a sense, these stationary waves, which include the Nusselt flat film as a stationary wave at all speeds c, are "fixed points" of the governing equations which are strictly unstable but the dynamics seem to approach them on a stable manifold and leave them rather reluctantly on an unstable manifold after a finite lifetime. The complete transition sequence then consists of evolution from one stationary-wave fixed point to another, possibly along a heteroclinic orbit. Such a scenario has also been envisioned for other instabilities. For example, stationary finite-

amplitude traveling waves are speculated to be the intermediate between the primary instability and the 3D tertiary phase in the transition sequence to turbulence in plane Poiseuille flow (Pugh & Saffmann 1988). The role of stationary waves is fully confirmed experimentally, however, on a falling film. This approach has spurred some recent activities to construct stationary wave families and analyze their stability. The latest results have already offered a good understanding of the evolution in regions II and III.

The last unique feature of wave evolution on a falling film is the dominance of the robust solitary-hump structure in the dynamics of regions III and IV. This feature promises to yield a very rational and quantitative description of the chaotic dynamics in these regions unavailable for turbulence in other instabilities. The existence of identical coherent units during spatio-temporal chaos in regions III and IV motivates a "coherent structure" theory describing the weak interaction among a finite number of such indestructible units. The dimension of the strange attractor in region IV, if the dynamics there is indeed governed by an attractor, can be relatively small. This is contrasted to the noise-like turbulence of high Reynolds number shear instabilities with continuous bands of length and time scales from unsynchronized waves and astronomical attractor dimensions. In this respect, "interfacial turbulence" in region IV of a falling film may indeed be related to low-dimensional chaos.

The next three sections summarize our current understanding of the transition sequence in Figure 1 and possible future development, especially along the line of "coherent structure" theory for the dynamics of regions III and IV. The dynamics of the inception region in I is well understood and we refer the readers to the earlier review of Lin (1983) and the latest computation of Floryan et al (1987). It should be mentioned, however, that although the linear dynamics at inception is clearly a convective instability, a complete confirmation of this has not been carried out. Pierson & Whitaker (1977) have computed the spatial amplification rate by presupposing the instability is convective. Most of the other literature on linear instability, beginning with the classical long-wave results of Yih (1963) and Benjamin (1957), actually pertain to the inappropriate temporal stability problem. The only attempts to ascertain convective instability are by Joo & Davis (1992b) and Liu et al (1992) who used the simplified equations of (1) and (2). However, their results yield a prediction of absolute instability at a sufficiently large R which has never been observed. The inconsistency was attributed to the failure of (1) and (2) in the absolutely unstable region. More precisely, it may be due to the missing high order (in ε) dispersion effect in these equations which becomes more pronounced at higher R. Since convective instability can be viewed as a competition between local growth and disturbance propagation, dispersion

of wave speed should have a profound influence on it. The erroneously predicted absolute instability is perhaps the linear precursor to the aphysical nonlinear blow-up behavior of (1). Both can then be attributed to the absence of dispersion in the equation. The inconsistencies of (1) and (2) with experimental data in this respect again limit their application. The confirmation of convective instability can be easily addressed by tackling the full Orr-Sommerfeld equation for the linearized Navier-Stokes equation or the linearized BL equation and this remains a worthy open problem.

We shall only cite a few important results from the linear study pertinent to subsequent discussion on nonlinear theories. These results remain valid in general despite their temporal stability formulation. Instability for the vertical film occurs beyond $R_c = 0$ and in an analog of Squire's theorem, the two-dimensional disturbances of the form $f(y)\exp(i\alpha x + \lambda t)$ are found to be more unstable than three-dimensional disturbances. The growth rate λ_r, shown in Figure 2, is a parabolic one that encompasses the range $\alpha \in (0, \alpha_0)$ where in the limit of low flow rate ($\delta \to 0$), the neutral wave number α_0 approaches $\sqrt{18\delta}$. Destabilization of long waves is due to gravity-driven inertia and stabilization of short waves is due to capillary effects. In the same limit of low δ, the fastest growing mode is $\alpha_m = \alpha_0/\sqrt{2} = \sqrt{9\delta}$, which seems to agree with the wave number of the naturally excited monochromatic wave emerging from region I. Again, a complete analysis of this linear filtering mechanism due to convective instability is still lacking. Also at low δ, the normalized phase velocity $c = -\lambda_i/\alpha$ is exactly 3 for all wave numbers α, e.g. all Fourier modes travel at three times the
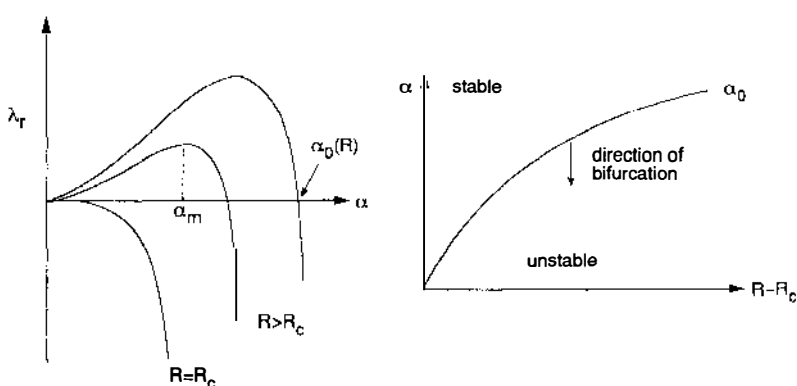

Figure 2 Schematic of the growth rate λ_r as a function of streamwise wave number α and the neutral curve for the neutral wave number α_0 as a function of Reynolds number R. The critical Reynolds number is R_c. The direction of bifurcation of the stationary periodic wave family is also indicated.

average velocity $\langle u \rangle$. With increasing δ, dispersion sets in and a mode near α_m travels slower than any other mode and is significantly lower than 3.

STATIONARY WAVES

Like other nonlinear theories for hydrodynamic instabilities, stationary waves and their stability can be studied with either a constant-flux or a constant-average thickness formulation. (These are analogous, but not identical, to constant-flux and constant-pressure-gradient formulations of other open-flow instabilities.) If a weakly nonlinear expansion about the flat-film is used, the latter formulation is usually implemented. For the full problem, however, either formulation can be used. The two results are qualitatively the same and quantitatively transformable (Chang et al 1993a).

The earliest attempts to construct stationary waves were by Benney (1966) for weak surface-tension fluids and Lin (1969) for strong ones. The constructed stationary waves are not necessarily the ones selected at the end of region II. Instead, they correspond to all possible stationary waves that are observed in a periodically forced experiment. Benney and Lin used the classical multi-scale formalism of Stuart-Watson to derive a Stuart-Landau (SL) equation

$$\frac{\partial a}{\partial t} = \lambda a - \sigma |a|^2 a \tag{5}$$

for the complex amplitude of a monochromatic wave with wave number α, $a \exp(i\alpha x)$. The complex coefficients λ and σ are simply the linear growth rate and the Landau interaction coefficient due to cubic self-interaction and quadratic interaction between the fundamental α and the overtone 2α. In the classical formalism, λ is expanded to leading order with respect to a bifurcation parameter like R at the maximum ("nose") of the growth rate curve near criticality $\lambda \sim (R - R_c)$ and σ is evaluated at the "nose." However, the growth rate of the falling-film problem in Figure 2 does not have a nose near criticality. More accurately, its nose at $\alpha = 0$ near criticality is too complex to allow an expansion that yields (5). As a result, (5) actually corresponds to an expansion carried out at the neutral curve and not at criticality, i.e. $\lambda \sim (\alpha - \alpha_0)$ and σ is evaluated at α_0 for all values of R and W. Hence, the solution of (5) is not limited to near-critical conditions as in other SL formulations. However, the most unstable waves near α_m of Figure 2 are not well-resolved at large R since $\alpha_m \ll \alpha_0$ at higher flow rates as the band of unstable waves grow with increasing inertia. This is

best clarified by a new derivation of (5) using modern Center Manifold theories (Cheng & Chang 1990). In the limit of small R (or δ), σ is a real parameter since the system is nondispersive. We also note that, by definition, λ_r vanishes at $\alpha = \alpha_0$ and is positive for $\alpha < \alpha_0$. The real part of the Landau constant σ_r is found to be positive, corresponding to a supercritical bifurcation, by all studies to date. This then implies that, at a given R and δ, there is a one-parameter family of nearly monochromatic periodic stationary waves parameterized by α with wave number decreasing continuously from α_0 (see Figure 2). The amplitude of each member of this wave family is given by $|a|^2(\alpha) = |\lambda_r(\alpha)/\sigma_r|$ which increases with increasing wavelength. The speed of each member is $-[\lambda_i(\alpha_0)/\alpha_0 - \sigma_i|a|^2/\alpha_0]$ where the second term represents the nonlinear correction to the linear phase speed $-\lambda_i/\alpha$ which is close to 3 at low R. Because the classical multi-scale formalism is extremely complex to apply, the computed speeds often deviated from investigator to investigator (Lin 1983). However, it is generally agreed that the nonlinear correction to speed is negative and longer waves tend to travel slower even though they have larger amplitudes. There were also attempts to construct stationary waves with wave numbers near zero, which are presumably near the infinitely long wavelength limit of the same wave family that begins at $\alpha = \alpha_0$. However, it is now known that the SL equation is only valid when the fundamental α is weakly unstable (i.e. just below α_0) while the overtone 2α is stable (Cheng & Chang 1990) and all prior results for α near zero such that $2\alpha < \alpha_0$ are incorrect. Even the maximum growing linear mode at $\alpha = \alpha_m$ is barely within this range and is hence poorly described by (5). Some investigators concluded correctly that whenever 2α lies within the unstable band of wave numbers in Figure 2, more than one amplitude equation must be considered because of the multiplicity of dominant Fourier modes. Lin (1974) suggested instead to use the long-wave evolution equations of (1) and (2) which can accommodate a large band of Fourier modes.

The first numerical studies of the stationary waves of the KS equation by Tsvelodub (1980), Demekhin (1983), Chen & Chang (1986), and Demekhin & Shkadov (1986) reveal the fate of the wave family that bifurcates off the neutral wave number at α_0 as predicted by the local analysis of the SL equation (5). As shown in the schematic of Figure 3, in the limits described by the KS equation, the wave family that bifurcates from α_0 is a standing wave family (5) with no nonlinear correction to the linear phase speed of 3. This is consistent with the local analysis of (5) since at low δ, σ_i vanishes and $-\lambda_i/\alpha$ approaches 3. The constructed amplitude is also in approximate agreement with the local theories of (5). However, at $(\alpha/\alpha_0) = 0.5547$, this standing-wave family undergoes a pitchfork bifurcation and yields two traveling-wave (relative to the linear phase speed)
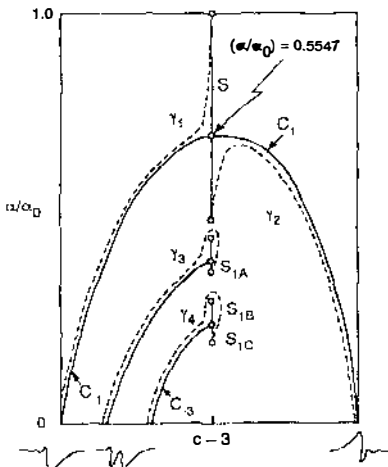
Figure 3 Schematic of the wave families of the KS equation in the wave-number/ speed $\alpha - c$ parameter space (*solid curves*). There is symmetry across $c = 3$ which is broken by inertia at finite δ (*broken curves*). Each wave family ends with a solitary wave at $\alpha = 0$ with different numbers of humps. The S wave families contain standing waves and the C families contain traveling waves of the KS equation. The γ families are the traveling waves at non-zero δ.

families $C_{\pm 1}$. This bifurcation is due to a "1-2 resonance" between the fundamental and its overtone which can be studied analytically if the amplitude equation of the now dominant overtone is added to the lone amplitude equation of the fundamental in (5) (Armbruster et al 1988). This bifurcation is hence beyond the description of the local Stuart-Landau equation (5). The two traveling-wave families are identical upon shape inversion ($\eta \to -\eta$) and reflection in space across the maximum ($x \to -x$) and in speed with respect to the linear phase speed [$c-3 \to -(c-3)$], transformations with respect to which the stationary KS equation with constant mean thickness

$$H_{xxx} + H_x - \mu H + 2H^2 = Q \qquad \langle H \rangle = 0 \qquad (6)$$

remains invariant. The constant $Q = \langle 2H^2 \rangle$ is the deviation flux and $\langle \ \rangle$ denotes a spatial average over one wavelength. The parameter μ is related to the deviation speed, $(c-3) \sim (8Q + \mu^2)^{1/2}$. [A convenient representation of the stationary wave solutions of (6) can be obtained by transforming (6) into a dynamical system $(x_1, x_2, x_3) = (H, H_x, H_{xx})$, such that $\dot{x} = f(x)$. In this formulation, the stationary waves become closed trajectories (limit cycles) in the three-dimensional phase space. Numerical construction is then achieved by using now-standard continuation routines to construct the limit-cycle branches and their bifurcations.] The two traveling-wave families, which possess stationary-wave members with a wide-band Fourier spectrum and speeds different from 3, then extend indefinitely to vanishing α without further bifurcations. The limiting wave member with an infinitely

long wavelength on the faster traveling-wave branch C_1 has a shape that has a striking resemblance to the solitary humps seen in regions III and IV of Figure 1. The limiting "negative" solitary wave on C_{-1} is inverted and reflected. Some members of these two families are shown in Figure 4.

All stationary wave families of the KS equation have now been constructed (Kevrekidis et al 1990, Demekhin et al 1991, Chang et al 1993a). There are actually an infinite number of such families. In the parameter space of μ and α, additional standing-wave families bifurcate from $\alpha = \alpha_0/n$, $n = 2, 3, \ldots$, as shown in Figure 5. Near the bifurcation points, they are identical to S and are, in fact, indistinguishable in the $c - \alpha$ bifurcation diagram of Figure 3. This is because a periodic standing wave with wavelength $2\pi/\alpha$ is also one with wavelength $2\pi n/\alpha$. However, further from the bifurcation points, they begin to deviate from S as perturbations much longer than $2\pi/\alpha$ are seen in the shapes (see the last wave family of Figure 4). Such distortions correspond to finite-amplitude manifestation of the classical subharmonic instabilities (Cheng & Chang 1992b) of the wave members on S and period-doubling in the dynamical-systems formulation. In the phase space, they correspond to a period-n limit cycle close to the period-1 limit cycle of S. All these subharmonic branches will undergo bifurcations to yield two symmetric traveling-wave families each as seen in Figures 3 and 5. These traveling-wave families terminate in solitary-hump-like waves in the vanishing-α limit but these limiting waves, in contrast to the one on C_1, have multiple humps. The faster multi-hump solitary waves are shown in Figure 6. (In Figure 3, the symmetry across $c = 3$ implies that whenever a family with speed slower than 3 exists, an inverted and reflected twin also exists with speed faster than 3. For clarity, only the slower twin is shown for some cases in Figure 3.) The n-hump solitary wave originates from the standing wave branch that bifurcates from $\alpha = \alpha_0/n$. It is convenient to use these solitary waves to represent the infinite number of traveling-wave families they head. They are not only physically important, as they resemble the humps seen in regions II and III, but also mathematically convenient since they allow the application of many new theories on homoclinic orbits.

It was realized recently (Pumir et al 1983) that the solitary waves correspond to homoclinic orbits in the phase-space formulation of any evolution and that the approach towards the solitary wave limit by the traveling-wave families in Figures 3 to 5 corresponds to a homoclinic bifurcation of a limit-cycle solution. Such homoclinic bifurcations and the resulting homoclinic orbits can be resolved *analytically* if the linearized Jacobian at the origin possesses eigenvalues close to two zeros with a geometric index of one (a double-zero singularity) or a zero and a purely imaginary conjugate pair (a $\{0, \pm i\}$ singularity). We (Chang 1986, 1987)
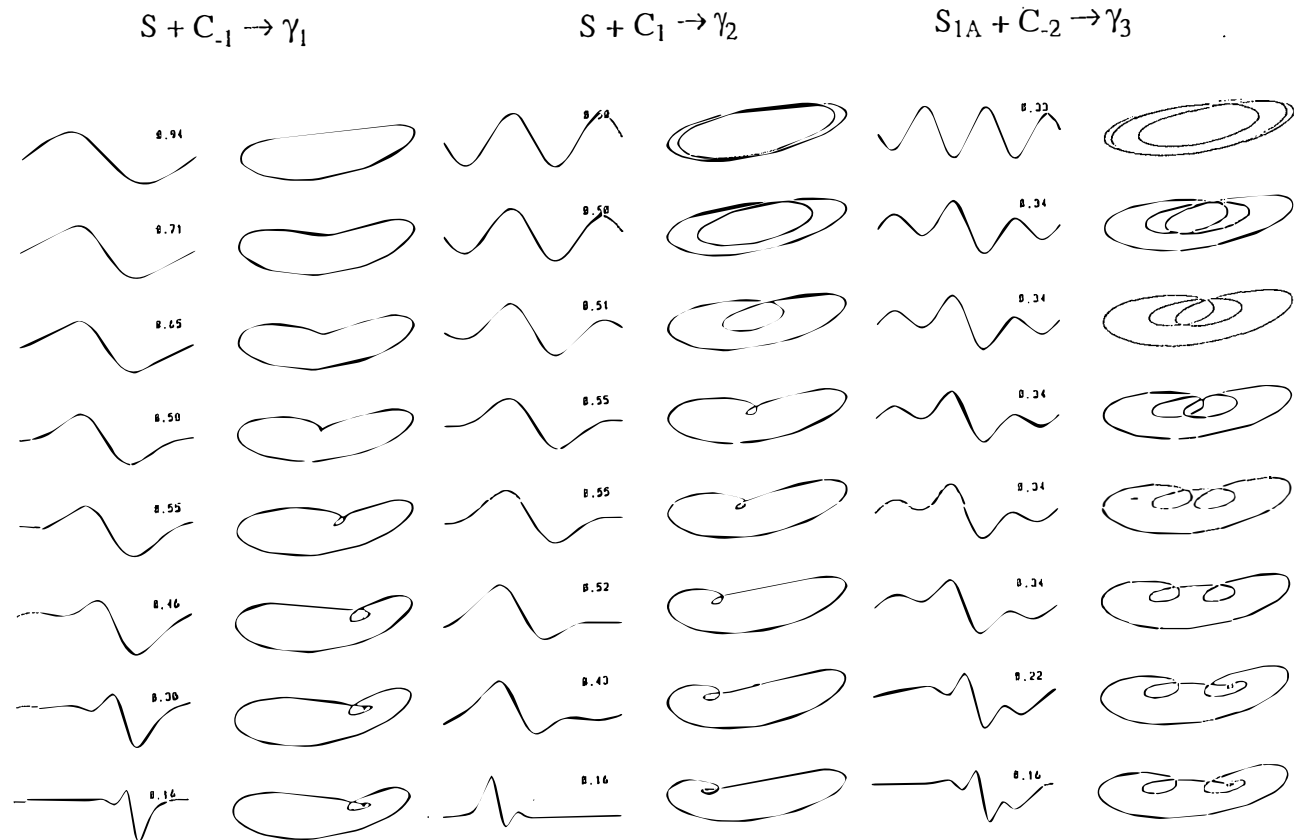
$$S + C_{-1} \rightarrow \gamma_1 \qquad S + C_1 \rightarrow \gamma_2 \qquad S_{1A} + C_{-2} \rightarrow \gamma_3$$

Figure 4   Individual wave members (wave tracings and phase-space trajectory analogs) of the γ_1, γ_2, and γ_3 families in Figure 3 from the BL equation at $\delta = 0.01$. The scales are not identical. The values of (α/α_0) are marked. The phase-space trajectories are also shown. The stationary waves range from a closed trajectory to a homoclinic orbit.
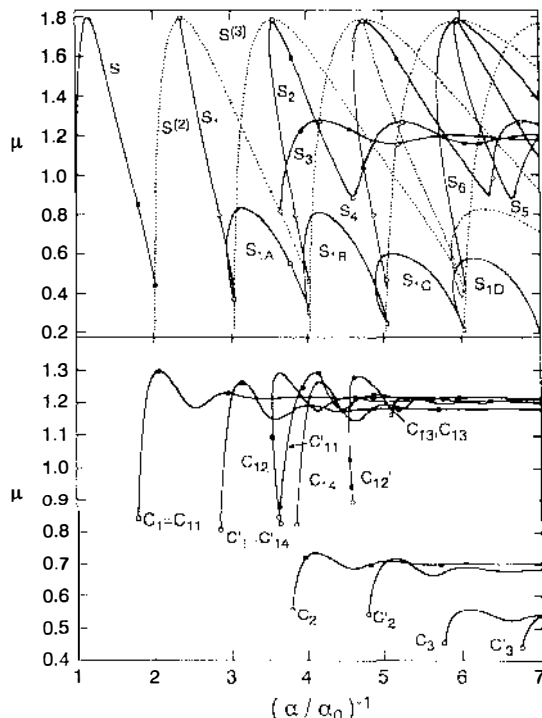
Figure 5 Fast wave families ($c > 3$) of the KS equation in the parameter space of $\mu - \alpha$ where μ is related to the speed and amplitude.

showed that for strong surface-tension fluids $[W \sim O(\varepsilon^{-2})]$, both (1) and (2) have eigenvalues close to the latter singularity if the speed c is close to 3. In this limit, the wave amplitude is small and both equations yield the same results. We carried out the necessary nonlinear coordinate transformation to convert the dynamical system into the normal form of that singularity. The lowest order nonlinear coordinate transformation smears the small differences in speed among the various small-amplitude solitary waves in Figure 5 and describes them as a continuous family of solitary waves parameterized by c. The resolution is also insufficient to distinguish the number of humps. Nevertheless, it yields the generic solitary wave shape shown in Figure 7. It corresponds to the homoclinic orbit shown in the same figure with a large loop followed by damped oscillations toward the fixed point connected to the loop. This corresponds to the gentle back and the steep front relaxed by the bow waves observed in the solitary humps of Figure 1. Since the bow waves correspond to local dynamics
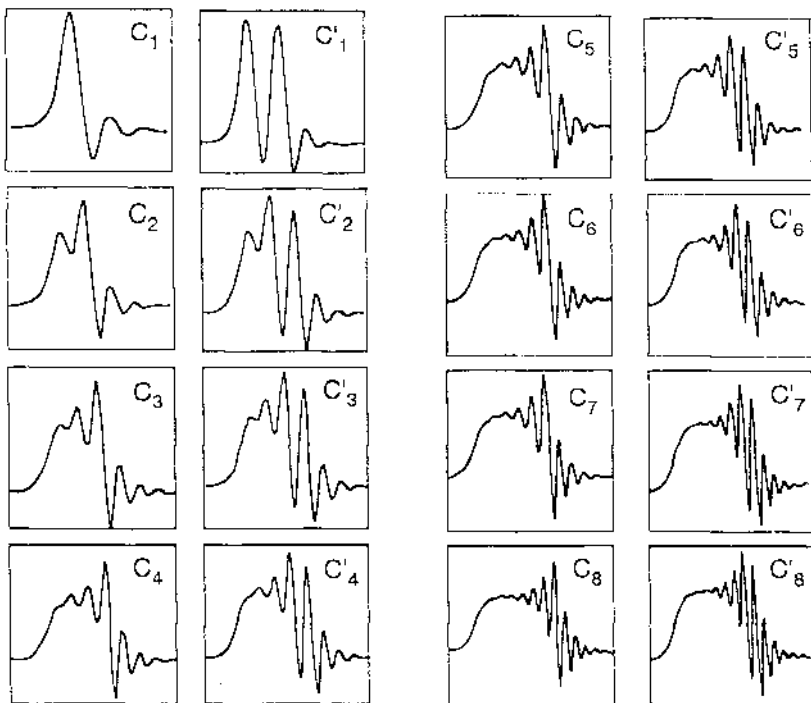
Figure 6 Multi-hump solitary waves which terminate the fast wave families ($c > 3$) of the KS equation at $\alpha = 0$. The traveling-wave family that each solitary wave belongs to is also indicated.

near the fixed point, a simple linear analysis shows that the bow waves have a wave number close to the neutral wave number α_0 which is in excellent agreement with experimental observation. Another interesting result is that the amplitude-speed correlation of all solitary waves or nearly solitary waves should be close to

$$c - 3 = 3(h - 1). \tag{7}$$

This simple prediction is consistent with the numerical result (Chang et al 1993a) and to the experimental speed and amplitude data of the solitary humps both in forced experiments and in regions III and IV of naturally excited waves as shown in Figure 7.

Recently, we have carried out a high-order resolution of the solitary-wave solutions (Chang et al 1993b) by adding a fictitious dispersion term to the KS equation,
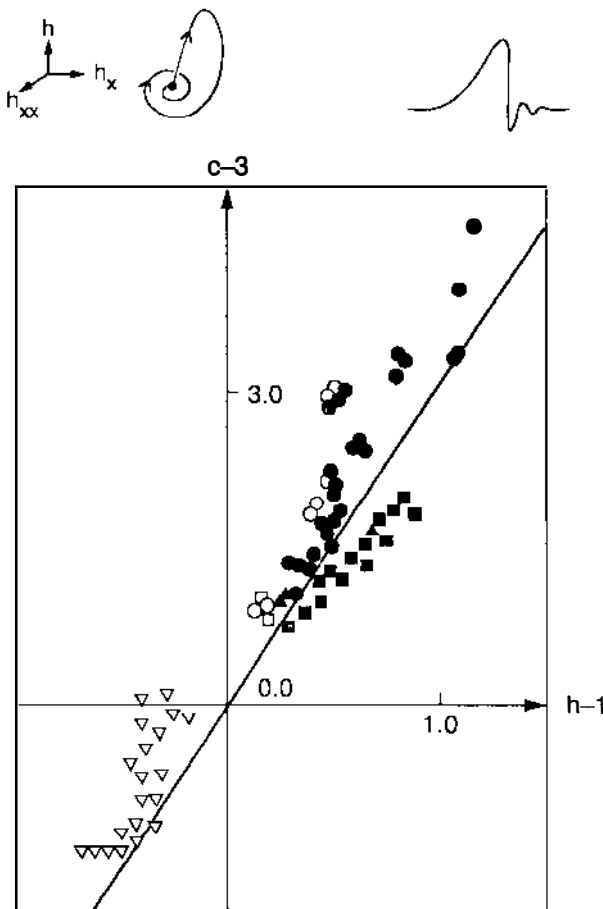
Figure 7   A solitary wave and its phase-space analog of a homoclinic orbit. Comparison of Equation (7) to the measured data of solitary humps (Chang 1986).

$$H_z + 4HH_x + H_{xx} + \delta' H_{xxx} + H_{xxxx} = 0. \tag{8}$$

(This equation can also be derived for inclined films with moderate surface tensions of a specific order.) With the unfolding provided by the additional dispersive parameter δ', the solitary-wave solutions indeed form a continuous family as shown in Figure 8. The limiting winding behavior near $\delta' = 0$ with a negligible distance between the speed c of individual solitary waves is the region we resolved earlier with our normal-form analysis which yielded Equation (7). For the KS equation with $\delta' = 0$, the solitary-
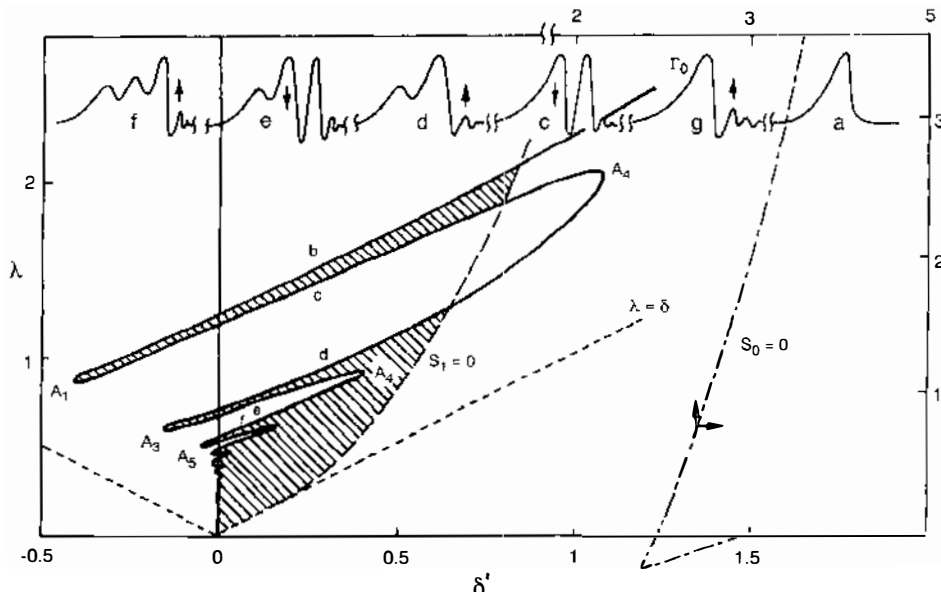
Figure 8 Unfolding of the solitary-wave solution branch of the extended KS equation of
(8) with a fictitious dispersion parameter δ'. The solitary wave structure at each branch is
also shown. The parameter λ is the deviation speed $\lambda \sim c - 3$. Intersections with the λ axis
correspond to solitary waves of the KS equation shown in Figure 6. The dotted lines and
shaded areas are related to the global Silnikov bifurcation that generates these solitary waves
(Chang et al 1993b).

wave members are discrete with the wave speeds forming a geometric series
with decreasing separation. Each member closer to $c = 3$ has an extra
hump corresponding to an additional traverse of the major loop in the
phase space of Figure 7. This sequence of solitary waves is also shown in
the vanishing α limit of Figure 3 and it corresponds to a peculiar bifurcation
of the homoclinic orbits related to the Silnikov mechanism (Glendinning
& Sparrow 1984). The primary solitary wave with one hump, cor-
responding to the limiting wave member of the traveling-wave family C_1,
has the largest speed of all solitary waves. It has a negative twin with an
inverted and reflected profile which is the slowest solitary wave. All other
solitary waves in Figure 8 can be considered as derivatives which bifurcate
off these two primary one-hump solitary waves. In fact, one can construct
the genealogy of the infinite number of wave families in Figures 3 and 5
by the following sequence of bifurcations. One begins with the one-hump
solitary wave of Figures 7 and 8. The speed and its shape are known in
detail (Toh 1987). Through a Silnikov bifurcation, unfolded by the fictional

dispersion term in Figure 8, it generates an infinite number of n-hump solitary waves. Each solitary wave then undergoes a reverse homoclinic bifurcation to generate a family of limit cycles (traveling waves). This sequence is followed in mirror image by the inverted twin of the primary one-hump solitary wave with the slowest speed. The one-hump twins are then the parents of all stationary traveling waves of the KS equation.

That the addition of dispersion can allow a more detailed resolution of the solitary waves is consistent with the analysis of the $O(\varepsilon^3)$ evolution equation of Nakaya for weak surface tension fluids (Chang 1989) which includes the higher-order dispersion effect in a rigorous manner. His equation was shown to be close to the double-zero singularity and the solitary waves form a continuous branch resolved by our analysis. It yields another amplitude-speed correlation for the near-solitary stationary waves which is also in favorable agreement with waves on glycerin or glycerin-water solutions. In general, the improved resolution of the stationary waves with the addition of either real dispersion or the artificial one in Equation (8) is consistent with our earlier discussions on the importance of higher-order terms like dispersion on linear instability and large-amplitude growth. To further support this, we point out that as δ approaches zero, the small-amplitude stationary-wave solutions of the BL equation collapse into the solutions of the KS equation and the small-amplitude waves of the evolution equation (1). However, the large-amplitude solitary-wave solutions of the strongly nonlinear evolution equation constructed by Pumir et al (1983) are not approached by the solitary waves of the BL equation in the same limit. This underscores the argument that the large-amplitude solutions of (1) are not correct because of the omission of dispersion and other high-order terms.

Most wave experiments for strong-surface-tension fluids like water are carried out in the intermediate-flow-rate region of $10 < R < 300$ where the KS equation is invalid. In this region, the BL equation (3) must be used and the elegant analysis available to the KS equation must now be replaced by brute-force numerical construction of the stationary waves. Nevertheless, many of the analytical and numerical results for the KS equation, which can be very clearly classified (for example, slow-fast symmetry and Silnikov bifurcations of solitary waves), are still useful in deciphering and organizing the bifurcations of the wave families of the BL equation from the KS solutions at vanishing δ.

The first attempts to construct finite-δ stationary waves focused on the ad hoc but simple IBL equation (Shkadov 1967, 1968; Demekhin & Shkadov 1985; Trifonov & Tsvelodub 1991; Tsvelodub & Trifonov 1992). The solutions are found to reduce to KS solutions at vanishing δ. However, some of the constructed wave shapes are not in good agreement with the

measured ones even at small δ values ($\delta > 0.05$). For the most common experimental conditions, only the IBL equation and the full Navier-Stokes equation are sufficiently accurate. While construction of stationary solution branches for the latter remain formidable, the former can now be analyzed completely to show good quantitative agreement with experimental data. We (Chang et al 1993c) have developed a spectral-element domain-decomposition numerical method for resolving the stationary waves of the BL equation. It is a routine specifically designed for the difficult free-surface problem of the falling film and we summarize below its resolution of the stationary waves.

At finite δ, the symmetries of the KS equation are broken and the pitchfork bifurcation of the standing-wave branch S which gives rise to the twin traveling-wave families becomes the imperfect pitchfork bifurcation shown in Figure 3. The standing-wave family S is linked with the slow primary traveling-wave family C_{-1} to form a new family γ_1. The primary fast traveling-wave family is isolated from this branch and forms γ_2. This perturbation of the pitchfork is also shown in Figure 4. As a result, the γ_1 family becomes a traveling-wave family with speed less than 3 and with wave number ranging from α_0 to zero. The segment of this slow wave family γ_1 near α_0 is the wave family resolved by the SL equation of (5). As shown in Figure 9, it is indeed slower than the linear phase speed due to nonlinear effects. The local resolution of the near-monochromatic waves by the Stuart-Landau equation is hence extended to the broad-banded stationary waves of Figure 11 at vanishing α. The γ_2 family, as shown in Figure 10, is a fast traveling-wave family with speed in excess of 3. This family could never have been resolved by local theories like the SL equation since it does not bifurcate off the neutral curve. Its wave number begins at $\alpha/\alpha_0 \sim 0.5$ and ends at $\alpha = 0$ in the positive one-hump solitary wave shown in Figure 7. The near-solitary waves ($\alpha \to 0$) of both the γ_1 and γ_2 families are still described by the analytical amplitude-speed correlation of Equation (8) up to $\delta = 0.3$. This is also confirmed in Figure 7 where the data correspond mostly to finite-δ values. Other pitchfork bifurcations of the subharmonic standing-wave branches are likewise broken to form an infinite number of traveling-wave families γ_i. However, as δ increases slightly from zero, these higher wave families begin to shift down in the $\alpha - c$ plane (as shown in Figure 9) and many of them actually coalesce and eliminate each other. By the moderate value of $\delta = 0.1$, corresponding to $R \sim 10$ for water, only a handful remain for $\alpha > 0.2$, including the primary γ_1 and γ_2 families. In fact, stability analysis described in the next section shows that the most stable (least unstable) waves of all branches lie only on the primary slow and fast families, γ_1 and γ_2, and the other wave families are essentially invisible. In retrospect, the two primary traveling
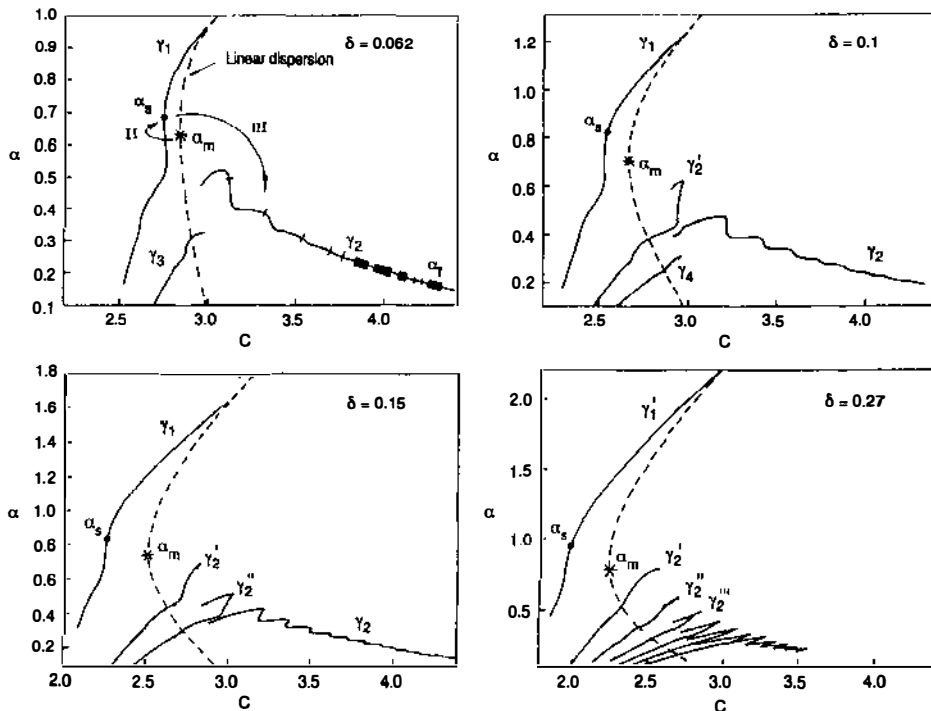
Figure 9 Actual wave families of the BL equation of various δ values. The top value of α in each figure corresponds to $\alpha_0 \sim \sqrt{18\delta}$. At moderate δ values, only the γ_1 and γ_2 families are important (See Figure 3 for the creation of these two families.) The narrow segments on these 2 families that are stable to two-dimensional disturbances are marked in the first figure. There is only one segment on γ_1, but multiple segments which correspond to a geometric series in α appear on γ_2. The wave transitions in a natural evolution are also marked. For $\delta > 0.09$, the high-α end of the fast γ_2 family degenerates into various families, none of which yield any stable segment.

waves $C_{\pm 1}$ of the KS equation, which arise due to a 1-2 resonance of the standing-wave family, and the two primary 1-hump solitary waves that terminate $C_{\pm 1}$ are actually the key stationary-wave families and solitary humps of the falling-film problem. The other infinite number of wave families are never reached in reality. This is hence a considerable simplification of the confusion of wave families shown in Figures 3 to 5. For $\delta > 0.09$, the short-wave (high α) end of the γ_2 family also undergoes a sequence of bifurcations which give rise to new γ_2^n families as shown in Figure 9. These new families are found to be extremely unstable, however. The long-wave end of the γ_2 family persists even at large δ and some
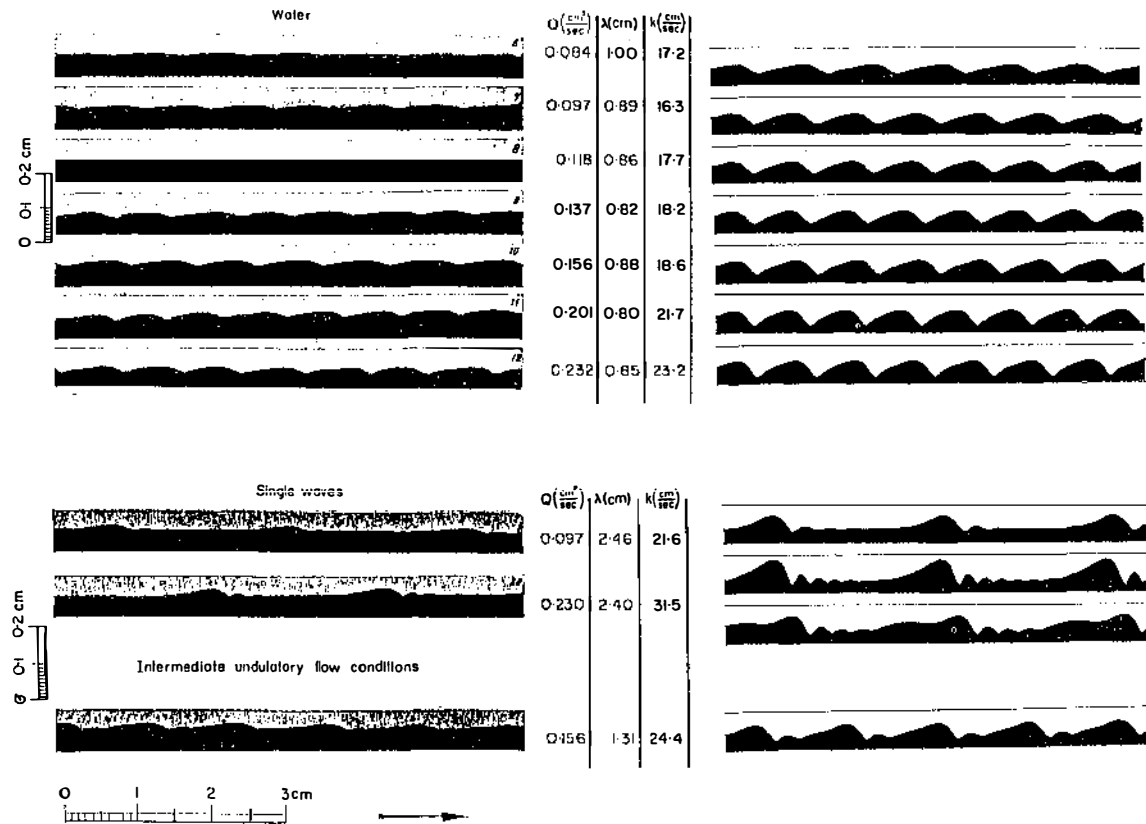
Water

$Q\left(\frac{cm^2}{sec}\right)$	$\lambda(cm)$	$k\left(\frac{cm}{sec}\right)$
0.084	1.00	17.2
0.097	0.89	16.3
0.118	0.86	17.7
0.137	0.82	18.2
0.156	0.88	18.6
0.201	0.80	21.7
0.232	0.85	23.2

Single waves

$Q\left(\frac{cm^2}{sec}\right)$	$\lambda(cm)$	$k\left(\frac{cm}{sec}\right)$
0.097	2.46	21.6
0.230	2.40	31.5
0.156	1.31	24.4

Intermediate undulatory flow conditions

0   1   2   3cm

Figure 10 Comparison of constructed γ_1 (*top*) and γ_2 (*bottom*) waves of the BL equation (*right*) to Kapitza's photographs of periodically excited waves of the same wavelength (*left*). The second tracing at the bottom shares the same wavelength with two constructed waves, one on γ_2 and one γ_2'.

selected waves, including ones exhibiting the characteristic solitary humps, are always found on the surviving segment.

The two primary families γ_1 and γ_2 are not only physically distinct in their speeds: In a constant-flux formulation, the slower γ_1 family has a smaller average thickness than h_N while the faster γ_2 has a larger average film thickness (Chang et al 1993a). (This is evident from the second γ_1 tracing and the first γ_2 tracing of Figure 10 which have the same flow rate.) This conclusion would seem counterintuitive unless one remembers that the waves are not mass-carrying—they travel faster than the fluid elements. Since region II in Figure 1 will be shown to contain γ_1 waves, this would imply that the averaged film thickness in region II is smaller than h_N if its flow rate is the same as in region I, i.e. the feed flow rate.

In Figure 10, some nearly monochromatic waves on γ_1 and some nearly solitary waves on γ_2 from our construction are compared to the classical photographs of Kapitza & Kapitza (1949) of the first waves generated by their periodically forced experiment. The waves are constructed to be the same wavelength as the observed ones. A slightly smaller amplitude is seen in the observed waves which can be attributed to the curvature effect of their cylindrical wall. Much better agreement is seen in Figure 11 where the forced-wave tracings from a more accurate measurement of Nal-
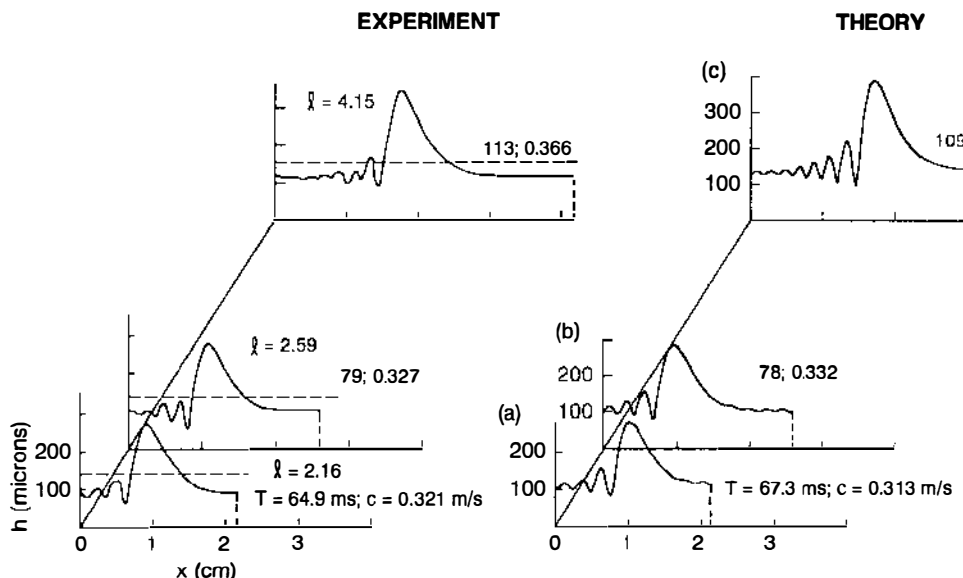

Figure 11   Comparison of constructed γ_2 waves to the ones recorded in the forced experiment of Nakoryakov et al (1985).

koryakov et al (1985) are used. Their waves are γ_2 waves generated by periodic forcing. Excellent agreement has also been found with the naturally excited waves measured by Stainthrop & Allen (1965). The inverted one-hump solitary waves on the vanishing α limit of γ_1 have never been recorded for a vertical film, but our constructed ones in Figure 4 resemble the waves measured by Liu et al (1993) for an inclined film. All measured stationary waves reported in the literature are in good agreement with the constructed ones from the BL equation (Chang et al 1993a).

WAVE SELECTION

P. Kapitza (1948) suggested at the very beginning that only some of the stationary waves generated by periodic forcing will be selected in a natural setting. All waves are expected to be unstable but the least unstable ones are presumed to be the chosen ones. He suggested a wave with the maximum absolute energy dissipation rate as the observed one. If the competing periodic stationary waves all have the same average thickness, which can be experimentally imposed, the selected one by Kapitza's criterion can be shown to carry the highest flow rate at low R (Chang et al 1993a). The earliest attempts to rigorize Kapitza's physical argument involved resolving the sideband stability of the near-neutral γ_1 waves estimated by the SL equation (5). The approach is to use the Ginzbury-Landau (GL) equation

$$\frac{\partial a}{\partial t} = \lambda a + \beta \frac{\partial^2 a}{\partial x^2} - \sigma |a|^2 a \tag{9}$$

by including the sideband effects in the complex coefficient β. However, as mentioned earlier, unlike other instabilities whose growth rate curve has a simple nose, the coefficients of the present SL equation are expanded about the neutral wave number α_0 and not at the nose near criticality. This implies that the linear growth rate has a nonzero slope $(\partial \lambda / \partial \alpha)(\alpha_0)$ and there should be a convective $\partial/\partial x$ term absent in the classical GL equation. Perhaps due to this, the GL equation (9) yields the erroneous prediction that slow γ_1 stationary waves near α_0 are stable to sideband disturbances which contradicts the recent experimental results of Liu et al (1993). A reexamination of the problem (Cheng & Chang 1992a), which uses center manifold techniques on the KS equation (2), reveals that, analogous to the Eckhaus bound for nondispersive GL equations, the near-neutral waves on the γ_1 (actually S) family are indeed unstable to sideband disturbances. The same waves have also been subjected to subharmonic instabilities by using the IBL equation for inclined films (Prokopiou et al

1991). Here, one needs to analyze the coupled fundamental and subharmonic amplitude equations (Cheng & Chang 1992b). The near-neutral waves on γ_1 are also found to be unstable to subharmonic disturbances. A more detailed analysis (Cheng & Chang 1993) has recently allowed us to compare these two dominant instabilities of the γ_1 stationary waves. It is found that the sideband instability is dominant near α_0 while the subharmonic instability takes over at a critical wave number below α_0. Our prediction agrees quantitatively with Liu & Gollub's experimental demarcation (1993) of these two instabilities. The boundary shifts down towards longer waves with increasing δ since the subharmonic instability is weakened by the detuning effect of dispersion (Cheng & Chang 1992b) while the sideband instability can be enhanced by dispersion (Cheng & Chang 1990).

We have extended the above stability analysis of γ_1 waves near α_0 by numerically imposing general two-dimensional and three-dimensional disturbances of arbitrary wavelengths in both the x and z direction to our constructed γ_1 waves (Chang et al 1993a). The resulting Floquet calculation confirms all the predictions of the local theories. Moreover, it shows that there is a finite-amplitude wave with wavenumber α_s on γ_1 (marked in Figure 9) that is the least unstable wave of the family. For small δ, this wave is actually stable to two-dimensional disturbances and only slightly unstable to three-dimensional ones. Beyond $\delta \sim 0.1$, however, it also becomes unstable to two-dimensional disturbances. Its growth rate never exceeds 30% of the dominant primary disturbance of the flat film at $\alpha = \alpha_m$ for $\delta < 3.0$. This confirms the long lifetime of the stationary waves. The dominant instabilities of this selected γ_1 wave are either a sideband mode $(\alpha_s \pm \Delta)$ or a subharmonic $(\alpha_s/2)$ in the x direction and a long transverse sideband instability in the z direction. Amazingly, Kapitza's criterion yields an accurate estimate of α_s at small δ after the viscous dissipation rate of our constructed waves is determined. This selected wave at α_s has a very physical characteristic—it is the wave with the highest flow rate (maximum dissipation) among all γ_1 waves in the constant-thickness formulation. It is a continuation of the stable segment at $(\alpha/\alpha_0) \in (0.77, 0.84)$ on the S family of the KS equation (Nepomnyaschy 1974, Demekhin & Kaplan 1989) which is actually stable to all disturbances. For all δ values, this selected wave has a wave number that is higher than the maximum growing linear mode α_m. This immediately suggests that a naturally excited wave which emerges with wave number α_m and the corresponding linear phase speed at the end of the inception region I will evolve in region II into a slower wave on γ_1 with a higher wave number α_s. This transition (shown in Figure 9) corresponds to a nonlinear deceleration and compression of the infinitesimally small wave field selected by the linear mech-

anism. The deceleration is qualitatively consistent with many observations (Lin 1983) and we (Chang et al 1993a) have obtained some quantitative confirmation with Stainthrop & Allen's (1965) wave speed data. Wave number data are, however, scarce and we verify the above transition scenario from region I to region II with a numerical experiment shown in Figure 12. We solve the initial-value problem of the BL equation in a frame moving at the linear phase speed to minimize wave translation. To bypass the long (in both space and time) inception region and to avoid boundary effects in the small computation domain, a small-amplitude
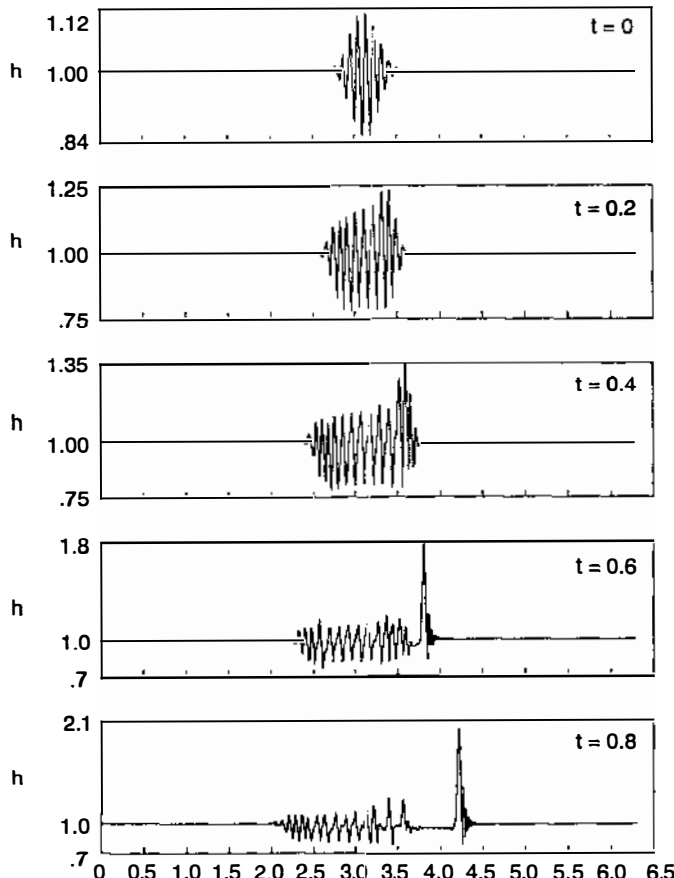
Figure 12 Numerical experiment on the transient evolution of a small-amplitude wave packet by using the BL equation at $\delta = 0.05$. The time scale t is actually stretched, αt, and the length scale αx.

wave packet with wave number close to α_m is inserted at the middle of the domain at $t = 0$. Our initial condition is hence spatially localized. The development of the overtone due to weakly nonlinear excitation is clearly visible at $t = 0.2$ and 0.4 as these waves form a lagging wave patch with more compressed waves. The wave number in this patch is close to α_s. If a uniform wave field could be used as the initial condition, one would see uniform compression and deceleration over a large domain.

We have also extended the stability analysis to the fast γ_2 waves and all other wave families. Here the Kapitza criterion is again found to be accurate at low δ. Interestingly, there are now multiple segments of local stability to two-dimensional disturbances on the γ_2 family as shown in Figure 9. These stable segments appear only at finite δ since the C_1 branch of the KS equation in Figure 3 is always unstable to two-dimensional disturbances. Members within these segments are again weakly unstable to three-dimensional disturbances that are sidebands or subharmonic in the streamwise direction and long sideband disturbances in the transverse direction. All other wave families are unstable to two-dimensional disturbances and hence are unlikely to be observed. The stable segments on γ_2 possess unique structures. The segment with the shortest waves is located near the turning point of the isolated branch γ_2 after the pitchfork is broken at $\delta = 0$. It hence possesses a wave number of about $(\alpha/\alpha_0) = 0.5$, i.e. the waves are twice as long as the neutral ones. They are much larger, longer, and faster than the waves near α_s on the γ_1 wave. Subsequent segments correspond to even longer and faster waves in the γ_2 family. As sketched in Figure 9, these narrow segments center at the wave number α_n and $|\alpha_{n+1} - \alpha_n|$ decreases geometrically as α_n decreases. For example, for $\delta = 0.062, \alpha_n = (0.48, 0.38, 0.31, 0.26, \ldots)$. An accumulation point α_f exists at about $(\alpha/\alpha_0) \sim 0.1$ for $\delta < 1.0$ below which the flat film between the humps becomes too long for the weak interaction between them to stabilize the flat-film primary instabilities of Figure 2. However, as shown in Figure 4, by $(\alpha/\alpha_0) \sim 0.2$, the periodic stationary waves in the γ_2 family have already taken on the shape of a solitary wave with the characteristic hump of Figure 7.

The important effect of dispersion is again seen here in the stability of γ_2 waves. The C_1 traveling-wave family of the nondispersive KS equation is unstable to even two-dimensional disturbances and yet its derivative γ_2 exhibits multiple stable segments with respect to the same disturbances. This is due to two effects, both related to the increased inertia in the BL equation. The destabilizing mechanism of inertia yields larger solitary humps which, in turn, intensify the interaction between humps that stabilizes the primary instability of the flat-film region between them. This interaction can be described with a coherent structure theory (Chang et al

1993a). However, the interaction between the solitary humps is stabilizing only if inertia-induced dispersion is present. This stabilizing effect of dispersion has been qualitatively confirmed by a recent study of the fictitious equation (8) (Chang et al 1993b). It was shown that not only does dispersion stabilize the long stationary waves, it also enhances their domains of attraction such that as δ' increases, more initial conditions approach the stationary waves corresponding to periodic trains of solitary humps. In the limit of infinite δ', (8) approaches the integrable KdV equation and periodic trains of its cnoidal solitary wave are approached for all initial conditions. The wavelength of the solitary wave train or correspondingly, the particular stable stationary waves on γ_2, is determined or selected by the initial condition. However, there is no question that, in the absence of transverse disturbances, stationary periodic trains of solitary humps will be selected if there is significant inertia-induced dispersion.

The stability analysis of the γ_1 and γ_2 wave families also suggests some possible scenarios for the transition from region II to region III in Figure 1. In essence, it corresponds to the system departing from the α_s wave on γ_1 to a stable one on γ_2. If significant transverse disturbances are present, this transition would lead to a stable wave on γ_2 with a wave number close to $\alpha_s/2$ since the most unstable three-dimensional disturbance has a subharmonic streamwise component. However, departure from α_s can also be triggered by finite-amplitude two-dimensional disturbances even when it is stable to infinitesimal two-dimensional disturbances at low δ. The most unstable (least stable) purely two-dimensional disturbance is often a sideband one and we would expect transition to a long wave in the γ_2 family. By the same token, if the domains of attraction of the stable waves on γ_2 are small, almost continuous transitions from one stable wave to another can be expected in the presence of finite-amplitude two-dimensional disturbances or three-dimensional disturbances. This is apparently the case but the observed transition in region III is not nearly as simple as the approach towards α_s in region II. The transition is first triggered by an intermittent and localized instability of the α_s wave which renders it difficult to discern a large patch of distinct periodic γ_2 waves. Consequently, the evolution along the γ_2 family towards the near-solitary wave at α_f tends to occur locally over one or two wavelengths rather than as a uniform wave field. Even in our idealized numerical experiment of Figure 12, each individual fast wave that leads the entire packet for $t > 0.6$ lies approximately within a different stable segment on γ_2. The large solitary hump that is dramatically emitted at $t = 0.6$ is close to the α_f wave of the γ_2 periodic stationary wave in Figure 4, suggesting an eventual evolution towards the solitary limit of this branch. The distinct difference in speed, shape, amplitude, and wavelength between this hump and the lagging wave

field underscores the distinction between the short γ_1 waves near α_s and the long γ_2 waves near α_f. Although this hump travels in a stationary manner and subsequent humps that leave the field are all almost identical to the first one, the separation between the humps is not uniform due to the intermittent nature of their creation process. We are unable to follow the humps further downstream to examine if they interact weakly with each other to form a periodic train or if the interaction remains nonstationary.

The more gradual and spatially uniform approach towards the α_s wave and the localized and intermittent departure from it are probably due to the different nonlinear mechanisms for the creation and destruction of the α_s wave. It is born by a short-range fundamental-overtone interaction involving only disturbances within one wavelength which are always present. Its death, on the other hand, requires long-range subharmonic and sideband streamwise disturbances which do not exist uniformly in space. Long-wave disturbances are definitely localized in our numerical experiment of Figure 12. Hence, coalescence of adjacent waves and long modulations tend to occur intermittently as localized defects. As a result, uniform γ_1 waves are observed during natural excitation while uniform γ_2 waves can only be observed with entrainment by periodic excitation. Even in the latter experiment, the primary instability of the flat film separating adjacent solitary humps prevents very long γ_2 waves to be sustained by periodic forcing (Alekseenko et al 1985, Liu & Gollub 1993). We (Chang et al 1993a) have shown that α_f is a good estimate of the lower bound on the wave number of the excitable γ_2 waves.

TURBULENT WAVE DYNAMICS AND FUTURE DEVELOPMENT

The only remaining wave dynamics that still escape understanding in this difficult but intriguing instability are the two-dimensional spatio-temporal chaos of region III and the three-dimensional interfacial turbulence of region IV. It is quite clear that the solitary-hump structures play an important role in these regions. It would be consistent with the underlying simple elegance of this difficult problem that the same solitary wave in Figure 7 that generates the infinite families of stationary waves via Silnikov and homoclinic bifurcations is also responsible for the turbulent dynamics. There are some preliminary results supporting this view. The long periodic stationary waves on the γ_2 family that are stable to two-dimensional disturbances must arrest the primary instability on the flat film region through a weak interaction of the two bounding solitary humps. This interaction is dominated by the small-amplitude ends of the solitary humps, the front bow waves of the back hump, and the smooth slope of the front

one (Kawahara & Toh 1988). In the phase space analogy, these two regions are described by the linear dynamics near the fixed point that the homoclinic orbit is attached to, and are hence easily deciphered by linear analysis. A weakly interacting coherent structure theory has been able to use these resolved ends to faithfully reproduce the sequence of stable wave segments on γ_2, including the geometric series in α (Chang et al 1993a).

These stable segments are unstable to three-dimensional disturbances. Consequently, transverse variation should be included in the coherent structure theory. The wavy crests seen in regions III and IV correspond to the classical "phase instability" of fronts described by a nonlinear diffusion equation. (In the more extreme cases, the phase evolution of the front is described by the KS equation!) One can hence envision a set of coupled nonlinear diffusion equations for the position of the wave crests as a function of t, x, and z. The coupling between the destabilizing transverse variation and the stabilizing streamwise interaction between the humps is responsible for the nonstationary dynamics. It is quite possible that a statistical theory with only nearest-neighbor interaction is sufficient to describe the dynamics of the entire interface in region IV. Dispersion will again play an important role here as it does in determining the convective instability of the inception region, in arresting blow-up behavior to form saturated two-dimensional stationary waves and in promoting the stability of stationary waves, especially periodic trains of solitary humps. The nonstationary dynamics is likely due to a competition between dispersion for the stabilizing streamwise interaction and Rayleigh capillary effects near the crest which cause the transverse instability.

The construction of weakly interacting theory for the solitary humps is equivalent to a perturbation analysis of a homoclinic orbit. The homoclinic orbit corresponds to a single solitary hump and the perturbations come from neighboring humps and transverse variation. Such perturbations can be studied with the new technique from Dynamical Systems theory for bifurcations of a homoclinic orbit, such as the Melnikov and Silnikov theories. Bifurcations of a homoclinic orbit are known to yield horseshoe maps and chaotic dynamics. It is hence very likely that the irregular spatio-temporal dynamics of regions III and IV can be described by chaos theory. It would then offer a direct contact between hydrodynamic turbulence, albeit a low Reynolds number one, and low-dimensional chaos. Research in this direction should be very fruitful and exciting.

ACKNOWLEDGMENTS

been privileged to work with a group of uniquely talented colleagues and students on this subject. The contributions of E. A. Demekhin, M. Cheng, S.-H. Hwang, M. Sangalli, and S. Kalliadasis have been especially important and I would like to dedicate this review to them.

Literature Cited

Armbruster, D., Guckenheimer, J., Holmes, P. 1988. Heteroclinic cycles and modulated travelling waves in systems with O(2) symmetry *Physica D* 29: 257–82

Alekseenko, S. V., Nakoryakov, V. E., Pokusaev, B. G. 1985. Wave formation on a vertical falling liquid film. *AIChE J.* 31: 1446-60

Benjamin, T. B. 1957. Wave formation in laminar flow down an inclined plane. *J. Fluid Mech.* 2: 554-74

Benney, B. J. 1966. Long waves in liquid films. *J. Math. Phys.* 45: 150–55

Bertschy, J. R., Chin, R. W., Abernathy, F. W. 1983. High-strain-rate free-surface boundary-layer flows. *J. Fluid Mech.* 126: 443–61

Chang, H.-C. 1986. Traveling waves in fluid interfaces: normal form analysis of the Kuramoto-Sivashinsky equation. *Phys. Fluids* 29: (10) 3142–47

Chang, H.-C. 1987. Evolution of nonlinear waves on vertically falling films—a normal form analysis. *Chem. Engrg. Sci.* 42: 515–33

Chang, H.-C. 1989. Onset of nonlinear waves on falling films. *Phys. Fluids A* 1: (9) 1314–27

Chang, H.-C., Demekhin, E. A, Kopelevich, D. I. 1993a. Nonlinear evolution of waves on a falling film. *J. Fluid Mech.* 250: 433–80

Chang, H.-C., Demekhin, E. A., Kopelevich, D. I. 1993b. Laminarizing effects of dispersion in an active-dissipative nonlinear medium. *Physica D* 63: 299–320

Chang, H.-C., Demekhin, E. A., Kopelevich, D. I. 1993c. Construction of stationary waves on a falling film. *Comput. Mech.* 11: 313–32

Chen, L.-H., Chang, H.-C. 1986. Nonlinear waves on liquid film surfaces—II. Bifurcation of the long-wave equation. *Chem. Engrg. Sci.* 41: 2477–86

Cheng, M., Chang, H.-C. 1990. A generalized sideband stability theory via center manifold projection. *Phys. Fluids* 2: (8) 1364–79

Cheng, M., Chang, H.-C. 1992a. Stability of axisymmetric waves on liquid films flowing down a vertical column to azimuthal and streamwise disturbances. *Chem. Engrg. Comm.* 118: 327-40

Cheng, M., Chang, H.-C. 1992b. Subharmonic instabilities of finite-amplitude monochromatic waves. *Phys. Fluids A* 4: (3) 505–23

Cheng, M., Chang, H.-C. 1993. Competition between subharmonic and sideband secondary instabilities of film flows. Preprint

Chu, K. J., Dukler, A. E. 1974. Statistical characteristics of thin wavy films. *AIChE J.* 20: 695–706

Demekhin, E. A. 1983. Bifurcation of the solution to the problem of steady traveling waves in a layer of viscous liquid on an inclined plane. *Izv. Akad. Nauk SSSR, Mekh. Zhidk. Gaza* 5: 36-44

Demekhin, E. A., Kaplan, M. A. 1989. Stability of stationary traveling waves on the surface of a vertical film of viscous fluid *Izv. Akad. Nauk SSSR, Mekh. Zhidk. Gaza* 3: 34–41

Demekhin, E. A., Shkadov, V. Ya. 1985. Two-dimensional wave regimes of a thin liquid films. *Izv. Akad. Nauk SSSR, Mekh. Zhidk. Gaza* 3: 63–67

Demekhin E. A., Shkadov V. Ya. 1986. Theory of solitons in systems with dissipation *Izv. Akad. Nauk SSSR, Mekh. Zhidk Gaza* 3: 91–97

Demekhin, E. A., Tokarev, G. Yu, Shkadov, V. Ya. 1991. Hierarchy of bifurcations of space-periodic structures in a nonlinear model of active dissipative media. *Physica D* 52: 338–61

Floryan, J. M., Davis, S. H., Kelly, R. E. 1987. Instabilities of a liquid film flowing down a slightly inclined plane. *Phys. Fluids* 30: (4) 983–89

Glendinning, P., Sparrow, C. 1984. Local and global behavior near homoclinic orbits. *J. Stat. Phys.* 35: 645–96

Ho, L.-W., Patera, A. T. 1990. A Legendre spectral element method for simulation of unsteady incompressible viscous free-surface flow. *Comput. Methods Appl. Mech. Eng.* 80: 355–66

Joo, S. W., Davis, S. H. 1992a. Irregular waves on viscous falling films. *Chem. Engrg. Comm.* 118: 111

Joo, S. W., Davis, S. H. 1992b. Instabilities of three-dimensional viscous falling films. *J. Fluid Mech.* 242: 529-47

Joo, S. W., Davis, S. H., Bankoff, S. G., 1991. On falling film instabilities and wave breaking. *Phys. Fluids* A3: 231–32

Kapitza, P. L. 1948. Wave flow of thin viscous fluid layers. *Zh. Eksp. Teor. Fiz.* 18: 1, 3–28; also in *Collected Works of P. L. Kapitza,* ed. D. Ter Haar. Oxford: Pergamon (1965)

Kapitza, P. L., Kapitza, S. P. 1949. Wave flow of thin fluid layers of liquid. *Zh. Eksp. Teor. Fiz.* 19: 105–20; also in *Collected Works of P. L. Kapitza,* ed. D. Ter Haar. Oxford: Pergamon (1965)

Kawahara, T., Toh, S. 1988. Pulse interaction in an unstable dissipative-dispersive nonlinear system. *Phys. Fluids* 31: 2103–11

Kevrekides, I. Nicolaenko, B., Scovel, J. C. 1990. Back in the saddle again: a computer-assisted study of the Kuramoto-Sivashinsky equation. *SIAM J. Appl. Math.* 50: 760–90

Kheshgi, H. A., Scriven, L. E. 1987. Disturbed film flow on a vertical plate. *Phys. Fluids* 30: (4) 990–997

Lin, S. P. 1969. Finite amplitude stability of a parallel flow with a free surface. *J. Fluid Mech.* 36: 113–26

Lin, S. P. 1974. Finite amplitude side-band stability of a viscous film. *J. Fluid Mech.* 63: (3) 417–429

Lin, S. P., 1983. Film waves. In *Waves on Fluid Interfaces,* ed. R. E. Meyer, pp. 261–90. New York: Academic

Liu, J., Paul, J. D., Banilower, E., Gollub, J. P., 1992. Film flow instabilities and spatiotemporal dynamics. *Proc. First Expt. Chaos Conf.,* ed. S. Vohra, M. Spano, M. Shlesigner, L. M. Pecora, W. Ditto, pp. 225–39. River Edge, NJ: World Sci.

Liu, J., Paul, J. D., Gollub, J. P., 1993. Measurement of the primary instabilities of film flows. *J. Fluid Mech.* 220: 69–101

Liu, J., Gollub, J. P. 1993. Onset of spatially chaotic waves on flowing films. *Phys. Rev. Lett.* 70: 2289–92

Nakaya, C. 1975. Long waves on thin fluid layer flowing down an inclined plane. *Phys. Fluids* 18: 1407–12

Nakoryakov, V. E., Pokusaev, B. G., Radev, K. B. 1985. Influence of waves on convective gas diffusion in falling down liquid film. In: *Hydrodynamics and Heat and Mass Transfer of Free-Surface Flows,* pp. 5–32. Novosibirsk: Inst. Heat Phys., Siberian Branch USSR Acad. Sci. (In Russian)

Nepomnyaschy, A. A. 1974. Stability of wave regimes in a film flowing down on inclined plane. *Izv. Akad. Nauk SSSR,*
Mekh. Zhidk. Gaza 3: 28–34

Pierson F. W., Whitaker, S. 1977. Some theoretical and experimental observation of wave structure of falling liquid films. *Ind. Engng. Chem. Fundam.* 16: (4) 401–8

Prokopiou, Th., Cheng, M., Chang, H.-C. 1991. Long waves on inclined films at high Reynolds number. *J. Fluid Mech.* 222: 665–91

Pugh, J. D., Saffman, P. G. 1988. Two-dimensional superharmonic stability of finite-amplitude waves in plane Poiseuille flow. *J. Fluid Mech.* 194: 295–307

Pumir, A., Manneville P., Pomeau Y. 1983. On solitary waves running down an inclined plane. *J. Fluid Mech.* 135: 27–50

Rosenau, P., Oron, A., Hyman, J. M. 1992. Bounded and unbounded patterns of the Benney equation. *Phys. Fluid A* 4: (6) 1102–4

Roskes, G. J. 1970. Three-dimensional long waves on a liquid film. *Phys. Fluids* 13: 1440–45

Shkadov, V. Ya. 1967. Wave conditions in the flow of thin layer of a viscous liquid under the action of gravity. *Izv. Akad. Nauk SSSR, Mekh. Zhidk. Gaza* 1: 43–50

Shkadov, V. Ya. 1968. Theory of wave flows of a thin layer of a viscous liquid. *Izv. Akad. Nauk SSSR, Mekh Zhidk. Gaza* 2: 20

Shkadov, V. Ya., Kholpanov, L. P., Malyusov, V. A., Zhavoronkov, No, M. 1970. Nonlinear theory of wave flows of liquid films. *Teor. Osn. Khim. Tekhnol.* 4: 859–67

Stainthorp, F. P., Allen, J. M. 1965. The development of ripples on the surface of liquid film flowing inside a vertical tube. *Trans. Inst. Chem. Eng.* 43: 85–91

Toh, S. 1987. Statistical model with localized structures describing the spatio-temporal chaos of Kuramoto-Sivashinsky equation. *J. Phys. Soc. Jpn.* 56: 949–62

Trifonov, Yu. Ya, Tsvelodub, O. Yu. 1991. Nonlinear waves on the surface of a falling liquid film part I. *J. Fluid Mech.* 229: 531–54

Tsvelodub, O. Yu. 1980. Steady traveling waves on a vertical film of fluid. *Izv. Akad. Nauk SSSR, Mekh. Zhidk. Gaza* 4: 142–46

Tsvelodub, O. Yu., Trifonov, Yu. Ya. 1992. Nonlinear waves on the surface of a falling film part II. *J. Fluid Mech.* 244: 149–69

Yih, C.-S. 1963. Stability of liquid flow down an inclined plane. *Phys. Fluids* 6: (3) 321–34